Loads, Stresses, and deflections in Bicycle Frames

Article *in* The Journal of Strain Analysis for Engineering Design · October 1986

DOI: 10.1243/03093247V214185

4 authors, including:

Bodunrin adegboyega Adeyefa
Czech Technical University in Prague
4 PUBLICATIONS **137** CITATIONS

SEE PROFILE

LOADS, STRESSES, AND DEFLECTIONS IN BICYCLE FRAMES

P. D. SODEN *Department of Mechanical Engineering, UMIST*

M. A. MILLAR *Department of Civil and Structural Engineering, UMIST*

B. A. ADEYEFA *Department of Mechanical Engineering, UMIST*

Y. S. WONG *Department of Mechanical Engineering, UMIST*

A bicycle frame has been analysed as a three-dimensional framework and stresses and deflections predicted using a finite element computer program. Theoretical results for simple loading case were compared with strain gauge measurements in laboratory tests.

More complex loading cases representing common cycle racing situations were analysed. The largest stresses in the frame were bending stresses. Stresses in the region of 300–400 MN/m^2 were predicted in the down tube and right chain stay during starting and stresses of about 250 MN/m^2 at the front of the top tube and down tube during severe braking.

1 INTRODUCTION

Most modern bicycle frames have the simple form shown in Fig. 1. This shape emerged in about 1895 following several decades of vigorous development and evolution (1)†, and has remained basically unchanged since that time. The need for low weight coupled with high strength and stiffness has led to continuing trial and development of high performance materials for racing bicycles and detailed specification of the proportions of these machines (2)(3). Most of the development has been empirical. Some analytical work has no doubt been carried out by commercial groups but the results have not been widely disseminated. The object of this paper is to present a first attempt at a theoretical analysis of a conventional bicycle frame.

The method used for modelling the frame will be described and theoretical predictions of frame deformation will be compared with experimental results for some very simple loading cases. More complex and realistic types of loading which racing bicycles are likely to encounter will then be considered and the theoretical stresses and deformations predicted for such loading will be examined.

2 MODELLING THE FRAME

At first sight the conventional bicycle frame, Fig. 1, may appear to be a simple, almost triangulated structure with all its members lying roughly in one plane.

However, even a superficial examination immediately suggests that the group of four members consisting of the head tube, top tube, seat tube and down tube, Fig. 2, must be regarded as a rigid jointed framework. A typical frame consists of tubular steel members brazed into elaborate connecting lugs. The tubes are of various thicknesses and diameters and major members are frequently thickened (butted) near the ends. Some members are tapered and have elliptical cross sections and the front forks are curved.

Furthermore, some major loads, such as pedal and chain forces, discussed in more detail below, are offset from the plane which contains the main frame members. Clearly any reasonably realistic analysis must allow for these factors.

A preliminary study indicated that a mathematical model of the primary elements of the bicycle frame could be obtained using an existing finite element computer program developed in the Civil and Structural Engineering Department at UMIST.

The program has facilities for structural modelling, using linear bar elements and membrane plate elements. Only the former elements were used in the present work.

Fig. 1. A modern sports cycle

(Photograph by John Rigby, courtesy of Harry Hall Cycles, Manchester, England)

The MS. of this paper was received at the Institution on 18 September 1984 and accepted for publication on 20 February 1986

† *References are given in the Appendix.*

0309–3247/86/1000–0185 $02.00

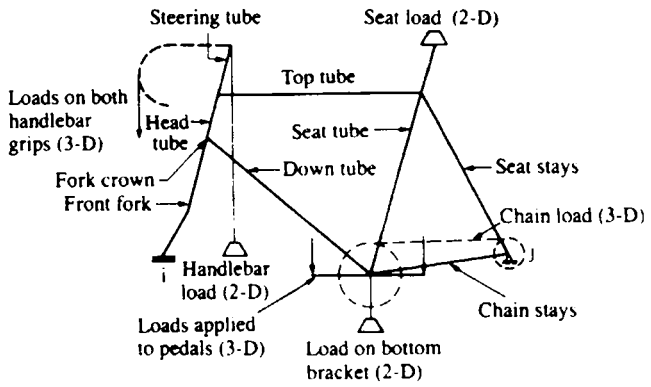

Fig. 2. Positions of application of loads during experiment

A feature of the version of the program used made it possible to investigate structures comprising rigid-jointed elements and pin-jointed elements, but not elements with a mixture of pins and rigid joints. The analyses were carried out assuming static loading, using stiffness equations based on small deflection theory.

2.1 The 2D model

As a comparison with earlier work, Amos (**4**), the bicycle was treated as a plane, rigidly jointed structure similar to the diagram in Fig. 2 in which the forks and the stays were represented by in-plane elements having twice the area and second moment of area of the actual members in the respective pairs. Loads were applied in the plane of the frame.

The lower end of the front 'forks' was free to slide horizontally, while the rear end (*j* in Fig. 2) was fixed in position but free to rotate.

For this plane '2D' model (model A) and all subsequent models, the lengths of the tubes covered by the lugs were each assumed to be equivalent to a small cylindrical member of the same outside diameter and overall length (measured from the tube centrelines) as the lug and the same internal diameter as the tube. Results show that the increased thickness at the lugs significantly stiffened the frame (**5**).

2.2 The 3D model

The frame model was subsequently developed to allow a more realistic three dimensional representation, incorporating the angle between the forks and stays and the plane of the main tubes of the bicycle and allowing out-of-plane loads to be applied.

An 88 element, 79 node model was used initially for the 3D modelling with some nodal points chosen to coincide with the positions of strain gauges installed on the frame, see Fig. 3. Additional elements and nodes were added to refine the mathematical model.

2.3 Modelling problems and constraints

There were two types of problems encountered in the modelling of the frame.

The first problem concerned the constraints between members, especially in the head tube assembly where the steering tube is connected to the head tube through bear-

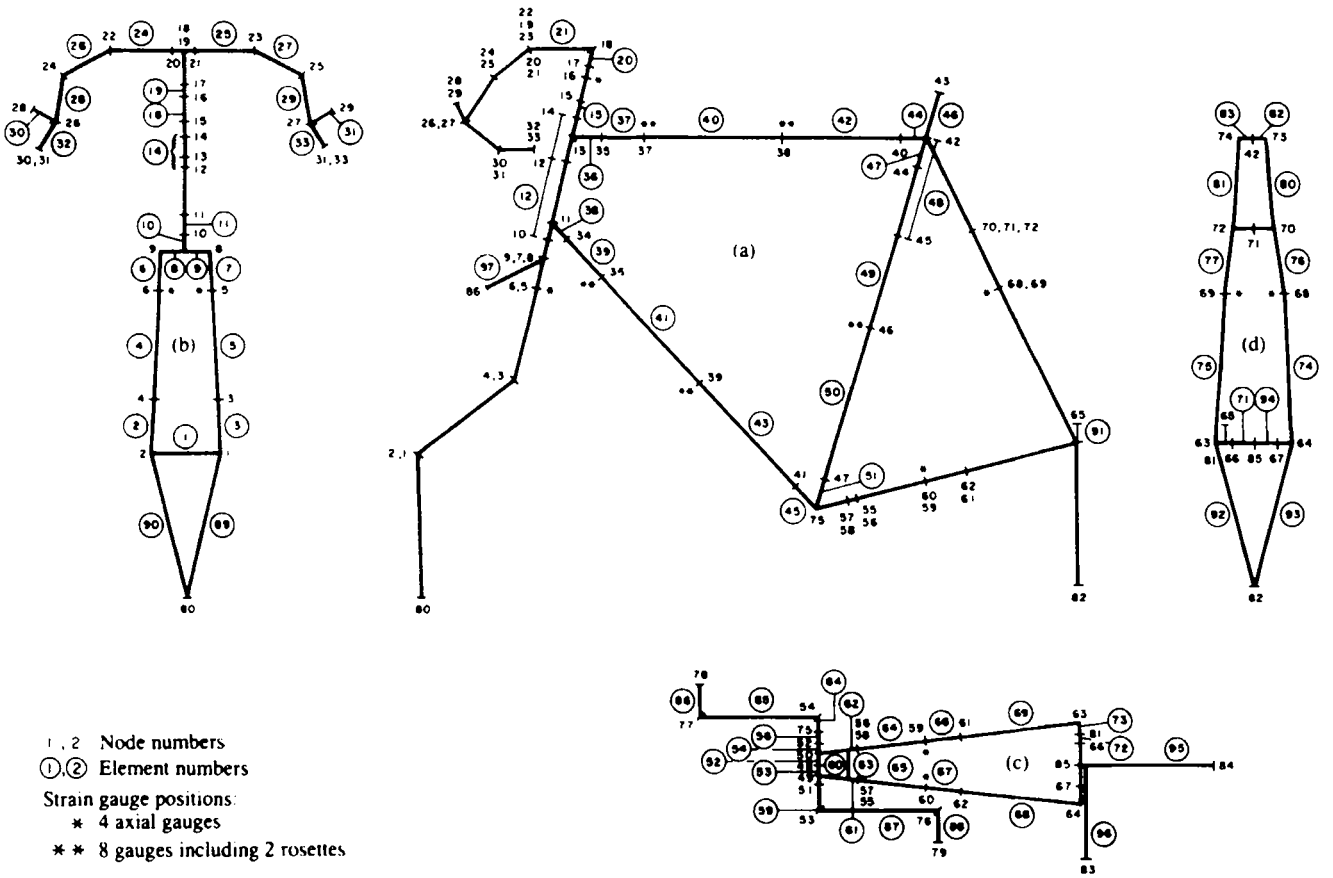

Fig. 3. Nodes and elements of the 3D models

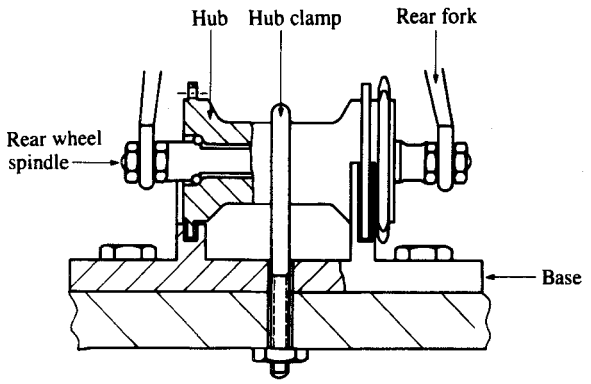

Fig. 4. Rear end mounting during laboratory tests

ings at two positions, and is thus incapable of transmitting torsion. This assembly was modelled using small intermediate members between the elements representing the two tubes. The intricate shapes of the fork crown and the lugs were approximated by simple shapes for the calculation of the areas and second moments of area.

The second and possibly the more important problem concerned the modelling of constraints at the hubs. For example, in actual riding conditions the rear hub and wheel spindle would be subjected to bending and twisting, as well as rigid body motion. The actual magnitudes of the deflections would depend, for a given load, on the stiffness of the wheel and the ground conditions.

In the first 3D model, two points on the rear hub spindle were fixed in position (nodes 66, 67, Fig. 3) while the rotation of the rear end of the frame was accomplished by the twisting of the protruding ends of the spindle (**5**). The chain load on the rear sprocket was applied at node 65. This model was chosen for two reasons: it obviates the need to know the wheel stiffness, and it corresponds closely to the configuration in the experimental set-up, Fig. 4. This 3D model was called model B. Obviously this arrangement introduces extra stiffness into the system due to the prevention of spindle deflection.

Another 3D model, model C, exactly the same as model B except at the rear constraint, was also considered. In this model, nodes 66 and 67 were freed and the forces at these points due to the bearing reactions were calculated and included in the revised data as input loads.

In analysing simple laboratory experiments it was not necessary to model the wheels, but in later attempts to simulate a freely moving bicycle, additional elements (element numbers 89, 90, 92, 93) were added to the model to represent the wheels (see section 5.1 and Fig. 3).

3 RESPONSE OF A FRAME TO SIMPLE LOADS

A bicycle frame was subjected to a series of simple loads in the laboratory. The measured deflections and stresses were compared with equivalent theoretical predictions, obtained as described in section 2.

3.1 Experiments

The bicycle was a 23 inch Holdsworth Record model in which the main tubes were made of chrome–manganese molybdenum steel (Reynolds 531). Thicknesses and major and minor diameters of the members were measured at 35 stations around the frame. Thicknesses were measured using an ultrasonic thickness gauge and checked against micrometer measurements where possible. The assumed material properties and typical measured thicknesses are given in Table 1, with full details in reference (**5**).

The wheels were removed and the frame was mounted on a rigid base. A large flanged hub was fitted to the ends of the front fork and rested on the horizontal top of the base. At the rear end, the hub was rigidly clamped to the top of the base with the spindle free to rotate within the hub. See Fig. 4.

Deflections at the front end and at the bottom bracket were measured with dial gauges while stresses were calculated from measured strain gauge recordings. The positions and arrangements of the strain gauges are indicated in Fig. 3. Some gauges were arranged at 45 degrees to the tube axes to measure shear strains. Each strain gauge was connected as an arm in a quarter-bridge circuit to a Peekel digital strain indicator (type PPE 815) through a Peekel strain gauge balancing unit (type PP2KRB1). A total of 64 strain gauges were used at 12 positions.

Loads were applied by 89.2N (20 lb) dead weights at the following positions (see Fig. 2):

Set a (3 separate loading cases)
(i) Vertical load on steering tube
(ii) Vertical load at centre of bottom bracket
(iii) Vertical load on seat

Table 1(a). Dimensions of main tubes

Member	Major dia. Minor dia. (mm)	Thickness (mm)
Seat tube	28.6	0.9
	28.6	
(at lug)	31.8	2.5
	31.8	
Top tube	25.4	0.7
(at lug)	29.02	2.5
Down tube	26.6	0.9
Head tube	31.75	0.9
Front fork	14.18	1.18
(76 mm from bottom end)	14.08	
(Top end)	28.72	1.20
	16.07	
Chainstay	23.1	0.79
(near bottom bracket)	21.8	
(near wheel)	16.1	1.03
	15.3	
Seat stay	11.3	1.27
(near wheel)	11.1	
(near seat)	16.4	0.98
	15.2	
Handlebar	23.7	1.96

Table 1(b). Material properties

Main frame members – steel, Renolds 531 (**10**)	
Young's Modulus:	200 GN/m^2
Yield stress (as drawn):	695 MN/m^2
after brazing:	618 MN/m^2
Tensile strength (as drawn):	772 MN/m^2
after brazing:	695 MN/m^2
Poisson's ratio:	0.3
Handlebars – aluminium alloy	
Young's Modulus:	7×10^{10} MN/m^2
Poissons' ratio:	0.33

Table 2. Deflections (mm) in in-plane (2D) model with lugs
Horizontal deflection – positive towards the rear of the cycle
Vertical deflection – positive upwards

Position of Dial Gauge	Position of vertical load					
	Handlebars		Bottom bracket		Seat	
	Measured	Computed	Measured	Computed	Measured	Computed
Front wheel (horizontal deflection)	−4.56	−4.04	−1.79	−1.62	−0.90	−0.86
Bottom bracket (vertical deflection)	−1.1	−1.07	−0.54	−0.54	−0.27	−0.29
Bottom bracket (horizontal deflection)	0.17	0.23	0.08	0.12	0.048	0.061

The vertical load is 446 N (100 lb) in each case.

Set b

(i) Vertical load on both handle bar grips
(ii) Vertical load on the centre of the left pedal (left crank was horizontal and forward, chain was placed over the 50 tooth chain wheel and 17 tooth rear sprocket)
(iii) Vertical load on right pedal, (right crank forward, horizontal, and chain engaged)

Since all the loads in Set *a* are in the plane of the frame, these experimental results are compared with those obtained theoretically using the 2D model.

On the other hand, some of the loads in Set *b* produce lateral bending and twisting of the tubes. The experimental results for the Set *b* load cases are compared with the results obtained for the 3D model in which the front fork ends were constrained to slide horizontally and the rear constraints were as for model B.

Before each run of the computer program the geometric input data was checked by plotting the shape of the frame on a visual display unit.

3.2 Comparison of experimental and theoretical results

There was reasonable agreement between the experimental and theoretical deflections for the 2D model, the largest difference being less than 12 per cent for deflections greater than ±1 mm, see Table 2. The level of agreement between experimental and theoretical axial loads and moments was not always as good, see Table 3. Some of the irregular discrepancies were due to erratic readings from particular strain gauges. For example, errors in gauge readings were responsible for the large difference between measured and computed axial forces at node 37 in the top tube when the force was applied to the handle bars.

Inaccuracies in measuring the frame dimensions, modelling of constraints, and the 2D modelling of the double members also contributed to discrepancies in forces and moments, such as the consistent errors in axial forces in the seat stays and moments in the front forks.

Load applied at the bottom bracket produced the largest loads in the main members and also the best agreement between experiment and theory.

Tables 4 and 5 indicate the differences between the 3-D model results and experimental results. All the deflections shown in Table 4 are of the correct order of magnitude and direction but discrepancies tend to be larger than before (Table 2). The maximum error shown in Table 4 was 1.44 mm, recorded at the front forks when

Table 3. Axial forces and moments – plane frame (2D) model with lugs
Load = 446 N (100 lb)
Forces – AF – Positive when member is in tension (N)
Moment – M – Positive when it causes clockwise rotation of left end of member (Nm)

Member	Position of Gauge *(node)	Axial force or moment	Position of load					
			Handlebar		Bottom bracket		Seat	
			Measured	Computed	Measured	Computed	Measured	Computed
Top tube	38	AF	−113.7	−127.8	−206.6	−208.5	−173.4	−113.2
		M	5.5	5.4	0.66	0.66	−0.13	−0.25
Down tube	39	AF	48.0	64.4	280.7	282.1	163	156.0
		M	13.7	11.4	2.94	2.60	1.58	1.44
Seat tube	46	AF	50.8	51.1	239.2	244.9	−210.5	−146.0
		M	−1.7	−1.9	−0.23	−0.51	−1.9	−1.4
Front forks	6	AF	−377.3	−329.7	−170.4	−170.4	−123.0	−74.2
		M	54.8	62.4	29.2	33.1	14.3	17.9
Down tube	36	AF	21.3	64.1	238.4	282.0	106.4	156.0
		M	44.7	35.1	8.4	7.6	2.5	3.6
Top tube	37	AF	−220.0	−127.8	−207.7	−208.5	−104.2	−113.2
		M	32.9	21.8	5.5	3.3	3.1	2.1
Chain stays	60	AF	27.7	57.8	113.5	128.6	189.8	164.4
		M	−4.5	−3.4	−0.41	−0.55	−0.55	−0.4
Seat Stays	68	AF	−183.0	−125	−346	−274.4	−441.4	−358.1
		M	−1.1	−1.1	−0.20	−0.58	0.80	0.51

* Refer to Fig. 3.

Table 4. Deflections (mm) using the 3D model

Magnitude of load (N)	115 on each grip		892		892	
Position of load	Handlebar grips		Left pedal		Right pedal	
Position of dial gauge	Exp.	Anal.	Exp.	Anal.	Exp.	Anal.
Front wheel Nodes 1, 2 – Horizontal deflection	−2.0	−1.56	−5.74	−5.78	−4.36	−5.8
Centre of bottom bracket Node 48 – Vertical deflection	−0.5	−0.64	−1.22	−1.87	−1.35	−1.93
Left end bottom bracket Node-51 – Vertical deflection	−0.5	−0.64	−1.87	−2.15	−0.6	−1.6
Node 51 – Horizontal deflection	0.1	0.14	0.4	0.42	0.25	0.25

Horizontal deflection – positive towards the rear ends.
Vertical deflection – positive upwards.

the load was applied at the right pedal. As the pedal loads are offset from the centreline of the frame the deformation in cases involving load applied to one pedal is more complex than before. For example, the displacements measured at the centre and end of the bottom bracket indicate the presence of bending and twisting of the frame.

Table 5 shows the theoretical forces in various members when a vertical load of 892N was applied at the centre of the left pedal together with measured forces derived from strain gauge readings. The results shown in Table 5 are typical of all results for Set *b* loading cases.

The causes of the differences between the theoretical and the experimental results must include the limitations of the theoretical models, some of which were mentioned earlier. However, the experimental set-up also introduced errors into the experimental results. Errors of about ±4 per cent arise from positioning and alignment of strain gauges and, more importantly, variations in readings of ±5 microstrain in each of the two gauges used for measuring axial forces and bending moments was estimated to produce an error of ±8 per cent in the value for the largest axial forces. On the whole a total error of ±12 per cent is expected from the experimental set-up, but considerably more in small readings. Much larger than expected experimental errors appeared to be present in some cases (see Table 5).

The errors in measured axial force and torque in the top tube are again associated with faulty strain gauge readings at node 37. The poor correspondence between theoretical and experimental shear forces is probably due to the low magnitude of the shear strains to be measured. Differences between the actual and model constraints probably contributed to the discrepancy between actual and theoretical axial forces and moments in the seat and chain stays which were particularly pronounced in the right seat stay.

A more detailed investigation would be necessary to identify all sources of discrepancy. For example, the source of error in the results for lateral bending moment at node 36 is unknown.

However, the theoretical models did predict the overall pattern of deflections, forces, and moments in the members. In all cases (see Tables 2–5) the theoretical

Table 5. Forces, moments, and torques in members for 892N vertical load at the centre of the left pedal. (Units: forces in N, moments in N/m)

Member	Node	Axial force	Shear force	Torque	M_v	M_w	
Top tube	38	−721.0	−43.5	3.47	2.20	−1.389	Analysis
		−719.6	−41.37	3.44	3.66	−0.787	Experiment
	37	−721.0	−43.5	3.37	11.34	−5.04	Analysis
		−485.2	−20.46	6.93	13.92	−5.59	Experiment
Down tube	39	976.0	−65.08	10.95	9.44	−7.14	Analysis
		967.1	−19.2	11.90	9.92	−9.33	Experiment
	36	974.3	−98.62	10.81	−30.22	3.66	Analysis
		1086.6	−4.7	10.58	−19.92	13.28	Experiment
Seat tube	46	848.2	28.53	1.39	−2.30	−27.79	Analysis
		601.9	74.16	0.25	−3.64	−39.01	Experiment
Front fork	5	−274.9			56.78		Analysis
(right)		−330.6			34.17		Experiment
(left)	6	−322.2			57.20		Analysis
		−359.6			35.46		Experiment
Seat stay	68	−930.5			−2.38	−5.33	Analysis
(left)		−1265.5			0.18	−5.95	Experiment
(right)	69	−17.8			1.01	2.47	Analysis
		344.7			0.537	7.12	Experiment
Chain stay	60	281.0			0.800	−6.41	Analysis
(left)		462.6			4.14	−10.76	Experiment
(right)	59	−1480.0			−5.67	−4.74	Analysis
		−1366.5			−4.24	−12.86	Experiment

M_v – moment in vertical plane through member.
M_w – moment in plane through axis of member, perpendicular to the vertical plane (see Fig. 9).

values at the different positions on the frame are of the same order of magnitude and in the same direction as the experimental results.

4 LOADS APPLIED TO A BICYCLE

4.1 Resistance and tractive forces

The loads applied to a bicycle by a rider during normal competitive cycling have been discussed in detail elsewhere (6). For a cyclist pedalling at a steady speed on level ground the resistance to motion is due mainly to aerodynamic drag and rolling resistance and these forces have been estimated from freewheeling and wind tunnel tests (2)(7). During hill climbing a component of weight acts down the incline and during acceleration and braking additional horizontal inertia forces are present which can be estimated if the rate of acceleration is known, (e.g., from cine-film records (5)(6)). The rider overcomes the total resistance to motion by applying loads to the pedals which are transmitted by the chain and sprockets to provide a horizontal tractive force at the rear wheel. If the resistance to motion and gear ratios are known the pedal forces which must be applied can be estimated (Table 6). Measurements (2) (6) (8) have shown that most of the pedal force is produced by pushing down on the front pedal, with maximum force being applied when the pedals are horizontal. Under some circumstances an additional pull is applied through the toe straps to the rear pedal.

Table 6 includes estimates of net (both feet) peak pedal forces produced by schoolboy riders during a variety of activities (5)(6). The large pedal loads developed during starting have been confirmed by measurements using an instrumented pedal (5).

The braking force in Table 6 was determined by calculating the horizontal force between the front wheel and the ground that would just produce overturning. In this case a coefficient of adhesion of 0.68 would be required between the tyre and the road to prevent the front wheel skidding, but this is possible on a dry road (2).

4.2 Forces applied to the bicycle

Riders tend to adopt different postures and styles under different circumstances. When riding on level ground they sit in a crouched position to reduce aerodynamic drag, but in situations such as hill climbing and starting, which require great effort, they tend to stand on the pedals and tilt the bicycle from side to side.

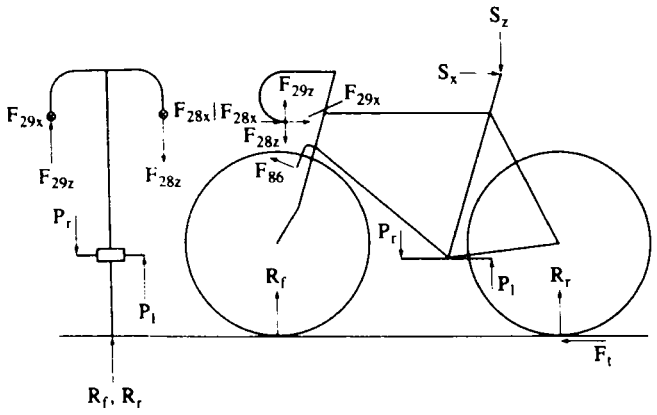

Fig. 5. Forces on the crank spindle

The position of the rider's centre of gravity can be estimated from photographs (5) and the quasi-static equilibrium equations for the cycle and rider together then allow wheel–ground reactions to be calculated. Using the simplified system of forces shown in Fig. 5 and the equilibrium equations for the bicycle alone, the individual pedal, saddle, and handlebar forces can be determined.

Estimated loads for a variety of common racing conditions are given in Table 7. In all cases the rider's body weight was taken as 660N, and loads were calculated when the cranks were horizontal. To simplify the frame loads, the weight of the bicycle was ignored. In each case it was necessary to neglect selected minor forces (see Table 7) to reduce the number of variables. Further details of the calculations are given in references (5) and (6).

Pedal forces in excess of bodyweight are achieved by pulling upwards on the handlebars and rear pedal (6). The pedal forces result in a lateral overturning moment which is resisted by pulling on one handlebar and pushing on the other, thus applying a twisting moment to the bicycle.

In all cases shown in Table 7 the handlebar forces are significantly large. The highest force levels considered were for starting. The forces were slightly larger when the

Table 6. Resistance and tractive forces

	Speeding on level ground at 37 km/hr	Climbing a 1 in 10 hill at 26 km/hr	Starting on level ground	Braking at 0.68 g
Aerodynamic Drag (N)	15	10	0	0
Rolling resistance (N)	9.5	8	0	0
Weight down incline (N)	0	66	0	0
Horizontal inertia force (N)	0	0	174	−449
Total tractive force (N)	−24.5	−84	−174	+449
Net max pedal force (N)	310	751	1813	0

+ ve backwards.

Table 7. Loads applied to the bicycle (N)

Position of load (ref. Fig. 5) \ Case	Speeding		Climbing (bicycle tilted)		Starting		Starting (bicycle tilted)		Braking	
	vert.* force (N)	force/aft** force (N)	vert. force (N)	force/aft force (N)	vert. force (N)	force/aft force (N)	vert. force (N)	force/aft force (N)	vert. force (N)	force/aft force (N)
Right pedal (P_r)	−310	0	−733	0	−1447	0	−1446	0	−119	0
Left pedal (P_L)	0	0	18	0	367	0	366	0	−119	0
Right handlebar (F_{29z}, F_{29x})	97	0	193	57	708	87	736	133	−86	−224
Left handlebar (F_{28z}, F_{28x})	−73	0	−138	17	−288	87	−316	41	−86	224
Seat (S_z, S_x)	−374	15	0	0	0	0	0	0	−250	0
Reactions										
Front wheel (R_f)	210	0	300	0	201	0	201	0	660	449
Rear wheel (R_r)	450	−15	360	−74	459	−174	459	−174	0	0
Resultant vertical force = weight of subject	660		660		660		660		660	

* +Ve upwards.
** +Ve backwards.

bicycle was tilted, but this is a rather artificial case because the bicycle is usually nearly vertical at the time when the cranks are horizontal (**5**).

The values of horizontal tractive force at the rear wheel shown in Table 7 are the estimated mean values for the various activities (as in Table 6, but excluding rolling resistance), while the pedal loads are estimated peak values taking into account the gear ratios selected by the rider and assumed patterns of torque variation throughout one revolution of the cranks. The maximum instantaneous tractive forces corresponding to the peak pedal forces would be higher than the mean values so that, strictly, all the horizontal forces for the speeding, climbing, and starting cases in Table 7 (and also in references (**5**) and (**6**)) underestimate the expected maximum values or imply higher gearing than was actually employed.

Dynamic wheel–ground forces arising from riding over rough ground may well be significant, but have been ignored in the present analysis.

4.3 Forces on the frame

The chain forces and hence the bottom bracket and rear wheel bearing forces (Figs. 6 and 7) were calculated from equilibrium considerations using pedal loads similar to those listed in Tables 6 and 7. To determine the forces applied to the front forks during braking of the front wheel it was necessary to consider equilibrium of the wheel and an additional element (97) was added to the model (Fig. 3) to transmit the force (F_{86} in Fig. 5) from the brakes to the frame.

All the derived forces acting on the bicycle frame during speeding, climbing, starting and braking for use with model B are listed in Table 8.

The effects of tilting the bicycle were simulated in two cases by adding lateral forces at the handlebars, pedals, and wheels.

The forces listed in Table 8 were based on data from Table 7. Figure 8 shows another set of forces for the case of starting with the bicycle vertical, including forces at the wheel bearings calculated for use with model C. The

Table 8. Forces applied to the bicycle frame (all forces N)

Member (node)†	Speeding			Climbing (bicycle tilted)			Starting			Starting (bicycle tilted)			Braking		
	X*	Y*	Z*	X	Y	Z	X	Y	Z	X	Y	Z	X	Y	Z
Front forks (1, 2) (2 off)	0	0	0	0	20	0	0	0	0	0	14	0	455	0	−87
R. Handlebar (28)	0	0	97	57	27	190	87	0	708	134	102	729	−224	0	−86
L. Handlebar (29)	0	0	−73	17	−19	−136	87	0	−288	40	−44	−312	−224	0	−86
Seat (43)	15	0	−374	0	0	0	0	0	0	0	0	0	0	0	−250
Bottom Bracket (51)	−184	0	484	−443	0	1179	−1082	0	−3198	−1070	0	3167	0	0	0
Bottom Bracket (52)	748	0	−755	1796	0	−1792	4378	0	−4047	4335	0	−4007	0	0	0
R. Sprocket (65)	−564	0	−39	−1353	0	−96	−3298	0	−231	−3265	0	−240	0	0	0
R. Pedal (78)	0	0	0	0	−102	0	0	0	0	0	−201	0	0	0	−119
L. Pedal (74)	0	0	0	0	3	0	0	0	0	0	51	0	0	0	−119
Front Brake (86)	0	0	0	0	0	0	0	0	0	0	0	0	−462	0	174

* Force directions are shown in Fig. 7.
Z – vertical, +ve upwards.
Y – lateral.
X – fore/aft +ve backwards.
† node positions are as shown in Fig. 3.

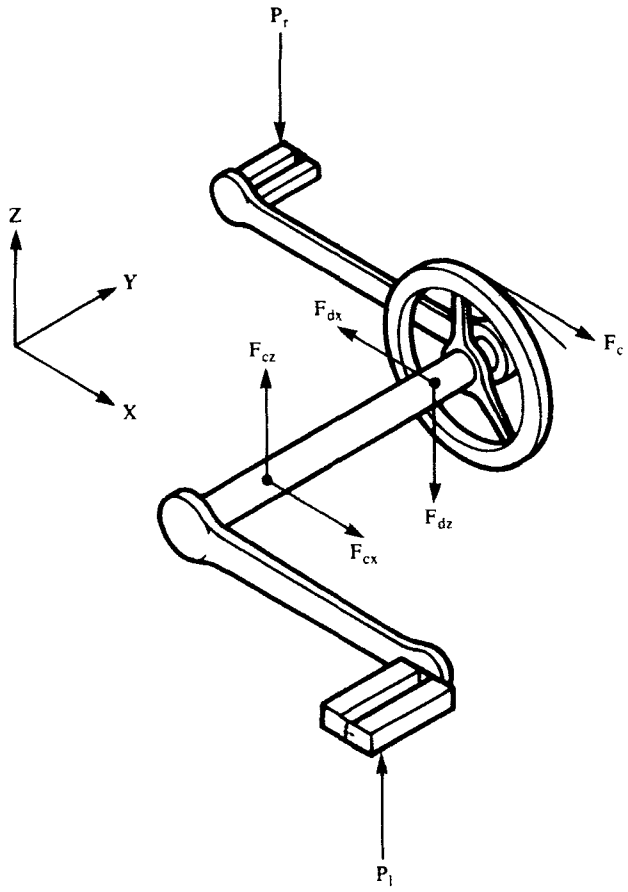

Fig. 6. Forces on the rear spindle

pedal and tractive forces (P_r = 1488N, P_L = 348N, and F_t = 313N) used for deriving this set of loads are all *peak* values, the tractive force being significantly greater than the corresponding mean tractive forces of Tables 6 and 7. A 42 tooth chainwheel and a 14 tooth rear sprocket were assumed.

5 THEORETICAL STRESSES AND DEFLECTIONS IN THE FRAME DURING NORMAL CYCLING

5.1 Nodes, loads, and constraints

The 3D models, models B and C were employed. The nodes in both models were as shown in Fig. 3.

The loads applied to model B were as shown in Table 8 and the loads applied to model C were as shown in Fig. 8.

To simulate the front wheel, the previous constraints imposed on the front fork ends were removed and two additional elements (89 and 90 in Fig. 3) were included in the model. The lower ends of these elements were fixed in position but free to rotate. In model B the rear spindle position was fixed at nodes 66 and 67, but for model C the stiffness of the rear wheel was represented by two elements (92 and 93) each of which was connected to a rear end node (63 or 64) and to the ground (node 82). Members 95 and 96 were introduced to take any unbalanced forces due to rounding errors, see Fig. 3.

5.2 Theoretical results

The ground reactions calculated by the computer program corresponded to the expected values and for

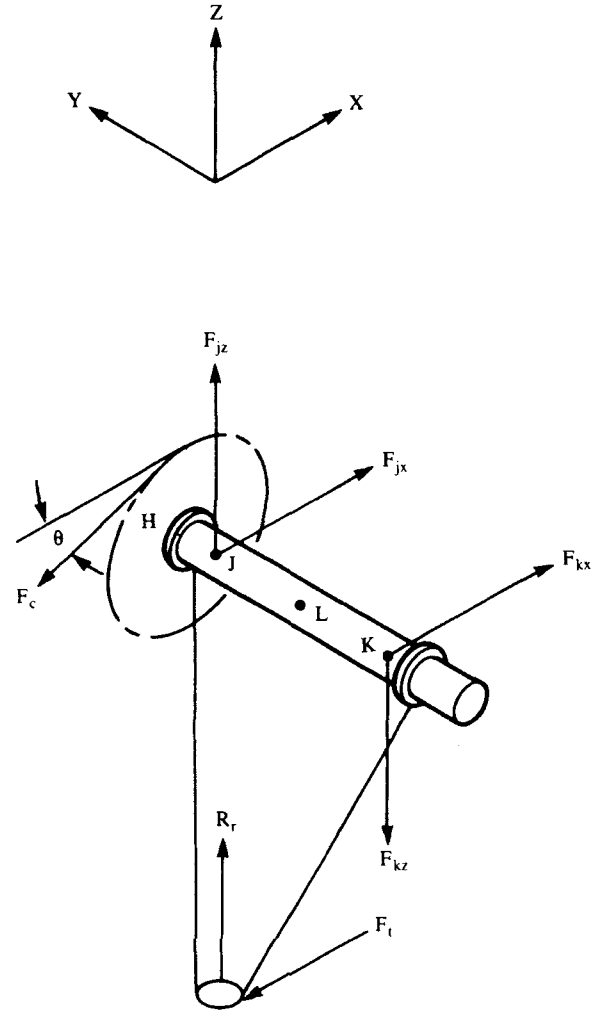

Fig. 7. Forces on the bicycle

model C the loads in the props (members 95 and 96 were negligible, confirming that the input loads were a self-equilibrating set.

Table 9 shows the predicted direct and bending stresses at selected nodes, for all loading cases considered using model B. On the whole, bending stresses were dominant, being much bigger than either the direct stresses or the shear stresses.

As expected in this type of structure the maximum bending moments and stresses occur at ends of members. Figure 9 shows a typical distribution of in-plane (M_v)

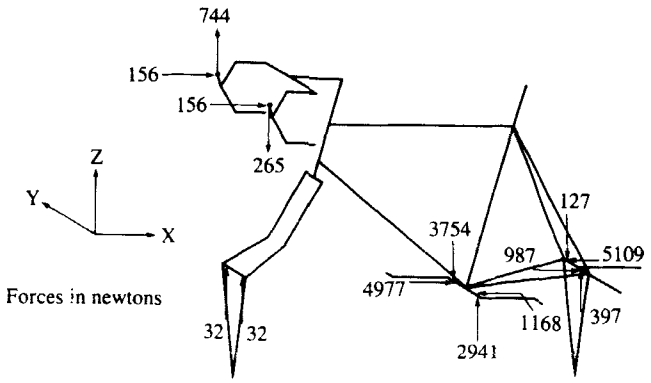

Fig. 8. Forces on the bicycle frame during starting (model C)

Table 9. Maximum stresses (MN/m^2)
Tensile stresses are positive. Bending stresses with asterisks (*) are due to M_v moments, the others are due to M_w moments

Member (node no.)	Speeding		Climbing bicycle tilted		Starting		Starting bicycle tilted		Braking	
	Dir.	Bend	Dir.	Bend	Dir.	Bend	Dir.	Bend	Dir.	Bend
Front fork (9)	−1	−35*	−1	−53*	−1	−33*	−1	−35*	−2	187*
Top tube (35)	−5	−30	−9	−93	−16	−174	−16	−174	5	236*
Down tube (34)	5	51	7	110	12	300	12	300	0	257*
Seat tube (47)	1	39	7	116	12	229	12	267	−2	91*
Chain stay (right) (58)	−9	−10	−24	−55	−63	−51	−61	−40	0	5*
Chain stay (left) (57)	1	8*	1	32	5	41	3	50	0	5*
Seat stay (right) (63)	−7	−10*	−10	−14	−8	−39*	−13	−32*	0	19*
Seat stay (left) (64)	−3	−10*	−3	−17*	−16	−87	−10	−51	0	19*

and transverse (M_w) bending moments in the main frame members. At the critical locations one of these bending moments was always much greater than the other. The bending stresses shown in Table 9 are those due to the larger of M_v and M_w.

When large loads are applied to one pedal as in the cases of speeding, climbing and starting, the lateral (M_w) bending moments in the main frame members were much larger than the in-plane (M_v) moments.

The largest stresses occurred in the case of starting, and tilting the bicycle did not significantly alter the distribution or the magnitude of the major stresses (see Table 9).

Because the pedal loads for the speeding, climbing, and starting cases were peak values, whilst tractive forces were mean values, the stresses shown in Table 9 are not exactly those that would be expected in practice. However, as will be shown for the case of starting, there is very little difference between the main tube stresses in Table 9 and those calculated taking both pedal and tractive forces as peak values with realistic gearing (Table 10).

In the case of braking, the loads applied to the left and right pedals were assumed to be equal and, hence, there

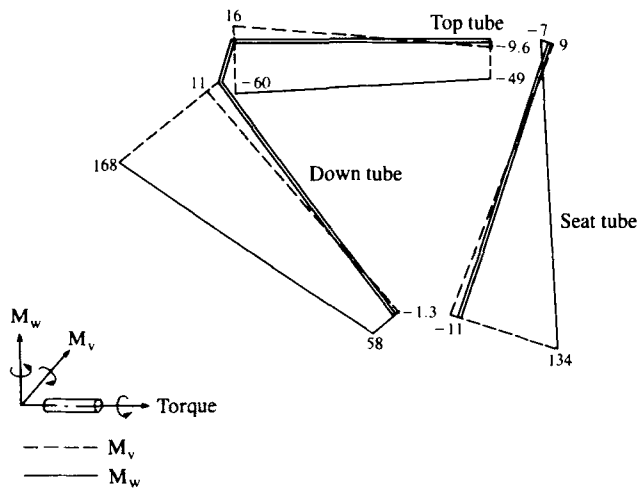

Fig. 9. Bending moment distribution in the main frame members during starting (model C)

was no lateral bending moment (M_w) in most members. However, the severe braking loads applied at the front wheel gave rise to very large in-plane bending stresses at the front end of the top tube and down tube (241 and 257 MN/m^2, respectively) and in the front forks (189 MN/m^2).

Of the cases considered in Table 9, only starting, with stresses of 300 MN/m^2 due to lateral bending at the top of the down tube, produced higher stresses than severe braking.

The starting case was investigated in more detail using the instantaneous peak forces shown in Fig. 8 and the model C which was considered to give most realistic modelling of rear wheel constraints. The resulting stresses due to direct and shear loads, in-plane and transverse bending moments, and torques at selected nodes are listed in Table 10.

The stresses (column 4 of Table 10) associated with shear loads were always very small. The direct stresses in column 3 were all smaller than the bending stresses (columns 6 and 7) and were insignificant, except possibly for the right chain stay. The shear stresses due to torsion (column 5) were also all smaller than the bending stresses.

The maximum axial stress (column 8) at each of the sections considered was obtained by adding the direct stress (column 3) to the maximum bending stress due to the resultant bending moment $\sqrt{\{(M_v)^2 + (M_w)^2\}}$.

The maximum principal stresses (column 9) were obtained by combining the maximum axial stresses from column 8 with the torsional shear stresses from column 5, ignoring the shear stresses from column 4.

The magnitude of the maximum principle stresses in the top tube, down tube, and seat tube in Table 10 are similar to those for the corresponding case in Table 9.

The largest stress for these members in Table 10 is the maximum principle stress (323 MN/m^2) at the front end of the down tube which is of very similar magnitude to its major component, the lateral bending stress (302 MN/m^2).

The largest of all the maximum principal stresses in Table 10 is 393 MN/m^2 at node 58 in the right chain stay. The largest component of that stress is again due to lateral bending, but nearly 20 per cent is due to a large compressive force of 3850N along the axis of the stay.

Table 10. Stresses in members during starting (model C).
Units MN/m^2. Tensile stresses + ve

(1) Member	(2) Node no.	(3) Direct stress	(4) Shear stress σ_D	(5) Torsion stress τ	(6) Bending σ_v (due to M_v)	(7) Stresses σ_w (due to M_w)	(8) Maximum axial stress σ_A	(9) Maximum principal stress σ_P
Right front fork	8	−0.04	0.16	—	13	2.7	−13	−13
Top tube	35	−16.2	3.7	53	47	174	−197	−210
Down tube	34	10.2	2.3	59	20	302	312	323
Seat tube	47	13.1	3.0	35	18	234	248	252
Right chain stay	58	−74.0	7.3	34	111	296	−390	−393
Left chain stay	57	3.02	4.6	34	79	256	271	276
Right seat stay	74	−0.98	1.47	5.2	21	55	−59	−60
Left seat stay	73	−19.3	1.02	3.9	15	47	−68	−69

Maximum axial stress $\sigma_A = \sigma_D \pm \sqrt{(\sigma_v^2 + \sigma_w^2)}$.
Maximum principal stress $\sigma_P = \sigma_A/2 \pm \sqrt{\{(\sigma_A/2)^2 + \tau^2\}}$.

This axial force is almost exactly equal to the chain force of 3824N.

While the slightly different loads in model B and model C must slightly alter the lateral bending moment (M_w) in the right chain stay, most of the increase is likely to be due to the modification of the restraint at the rear wheel.

5.3 Comments on the results

The maximum stresses calculated for the starting and severe braking cases are quite high. In the case of starting, the maximum stress is about 60 per cent of the yield strength and more than 50 per cent of the tensile strength of Reynold 531 tubing (see Table 1(b)). The loads used in the calculations were derived from experiments using extremely fit young riders (**6**). Trained adult riders might be expected to apply larger loads, but not necessarily in proportion to their bodyweight. It is unlikely that loads of the type and magnitude we have considered would cause yielding or fracture of the frame if good quality steels are used throughout and the loading is only repeated a small number of times. There is, of course, a possibility of fatigue in any component that is subject to repeated load. As a rough guide, the endurance limit for polished steel specimens, without stress concentrations, subjected to reversed bending can be taken as approximately 50 per cent of the tensile strength (**11**).

If the high loads described previously were repeated very frequently, fatigue failures would occur. We have no data on the frequency with which racing starts and emergency stops are performed, but, provided they do not occur more than a few thousand times, fatigue failures from that source are not expected to be a serious problem. Some loads could be repeated frequently. For example, the loads arising from the 'speeding' case would be applied with each revolution of the crank. Note, however, that the magnitude of these loads was significantly lower than the loads predicted during starting. Any attempt to predict fatigue life would require additional information including data on the magnitude and frequency of the various types of loading expected and evaluation of local stress concentrations that could occur at lugs and elsewhere.

Twisting of the frame by lateral bending of the members has been identified as a major form of loading and more attention could be paid to reducing weight by reducing lateral bending stresses. For example, the effect of using more double frame members could be evaluated.

The large deflections noted during starting suggest that some of the rider's effort is being used in deforming the bicycle frame. Further work is required to evaluate the magnitude of these losses and establish means of increasing lateral stiffness if that is found to be desirable.

There may be other riding conditions which produce higher tube stresses than the cases considered here. In particular the influence of dynamic loading due to rough and bumpy roads could be significant.

6 CONCLUSIONS

It has been shown that the stresses and deflections of a bicycle frame due to loads applied during riding can be calculated using the finite element method.

The largest stresses in the frame tubes are due to the lateral bending caused by the out-of-plane forces, applied through the handlebars, the chain, and the pedals, and due to in-plane bending during braking.

Of the four cases considered, the maximum stresses of 393 MN/m^2 and 323 MN/m^2, respectively, occurred at the bottom bracket end of the right chain stay and at the top end of the down tube for a net load of 1835N on the pedals during starting on level ground. Violent braking of the front wheel produced stresses of up to 257 MN/m^2 at the front end of the down tube and top tube due to large bending moments applied to the front forks.

A more detailed study would be necessary to quantify the various sources of discrepancy between experimental and theoretical results shown in Tables 2–5.

The techniques provide a promising method of evaluating alternative frame designs.

More attention could be paid to designing frames to resist bending due to the offset loads.

APPENDIX

REFERENCES

(1) SHARPE, A., *Bicycles and tricycles*, 1896 (Longmans Green, Cambridge, MA). Reprinted 1977, MIT Press.
(2 WHIT, F. R. and WILSON, D. G., *Bicycle science*, 1974 (MIT Press, Cambridge, MA and London).
(3) WATSON, R. and GRAY, M., *The Penguin book of the bicycle*, 1978 (Penguin London).
(4) AMOS, A. R., *A preliminary investigation into cycle frame design*, 1977, BSc project report, Department of Mechanical Engineering, UMIST.

(5) ADEYEFA, B. A., 1978, *Determination of load deflections and stresses in bicycle frames*, 1978, MSc Dissertation, UMIST.
(6) SODEN, P. D. and ADEYEFA, B. A., 'Forces applied to a bicycle during normal cycling', *J. Biomech.*, 1979, **12**, 527–541.
(7) KYLE, C. R. and EDELMAN, W. E., 'Man powered vehicle design criteria', presented at the 3rd Int. Conf. on Vehicle System Dynamics, Blackburn, Virginia, USA, 12–15 August, 1974.
(8) HOES, M. J. A. J. M., BINKHORST, R. A., SMEEKES-KUYE, A. E. M. C. and VISSERS, A. C. A., 'Measurements of forces exerted on pedal and crank during work on a bicycle ergometer and different loads', *Physioleinchl. Arbeitsphysiol.*, 1968, **26**, 43–94.
(9) WONG, Y. S., *Computer aided design of bicycle frames*, 1979, BSc project report, Department of Mechanical Engineering, UMIST.
(10) Reynolds Tube Co. Ltd., 'Material data sheet No. T204, Birmingham, England.
(11) SHIGLEY, J. E., *Mechanical engineering design*, (3rd edition), 1977 (McGraw-Hill, New York).